AIAA JOURNAL
Vol. 36, No. 6, June 1998

Experimental and Numerical Study of Supersonic Film Cooling

B. Aupoix,* A. Mignosi,† and S. Viala‡
ONERA, 31055 Toulouse Cedex 4, France
and
F. Bouvier§ and R. Gaillard§
ONERA, 92190 Chalais–Meudon, France

An experimental study has been performed at ONERA to simulate film cooling in a rocket engine. Two injector heights and cold and ambient temperature films, as well as matched and under- and overexpanded films, have been investigated. The mixing process has been documented by measuring the Mach number and temperature profiles. In addition, wall pressure and temperature, as well as heat transfer coefficients, have been measured. A boundary-layer code has been used to compute this flow. To achieve a fair prediction of the flow, several turbulence models, including compressibility corrections, have been tested. The prediction of the mixing-layer expansion is crucial for the quality of the computational results. We have concluded that the algebraic models tested are not suitable to compute this flow and that the best agreement is achieved with the model of So et al. (So, R. M. C., Zhang, H. S., and Speziale, C. G., "Near-Wall Modeling of the Dissipation-Rate Equation," AIAA Paper 92-0441, Jan. 1992).

Nomenclature

a	= speed of sound
h	= heat transfer coefficient, $\Phi_w/(T_w - T_{\text{eq}})$
k	= turbulent kinetic energy
M_c	= convective Mach number
p	= pressure
T	= temperature
U	= velocity
x	= streamwise coordinate
y	= coordinate along the wall normal
δ'	= mixing-layer expansion rate
ε	= turbulent kinetic energy dissipation rate
λ	= mass flow ratio
ρ	= density
Φ	= heat flux
ω	= specific dissipation, ε/k

Subscripts

eq	= equilibrium value
i	= stagnation value
inc	= incompressible value
j, f	= film value
m, 0	= main flow value
w	= wall value

I. Introduction

In future versions of the Vulcain rocket engine for the Ariane 5 cryogenic main stage, it is planned to inject the turbine exhaust gases in the rocket nozzle. The objectives are to better use their contribution to the thrust and to cool the nozzle.[1] A tangential film is injected to protect the wall from the hot flow. The fully protected region is the region downstream from the injection where the wall temperature or the wall heat flux is only governed by the film behavior. Farther downstream, the hot flow diffuses down to the wall, causing the film to break. Supersonic film injection is known to give little mixing between the film and the main flow, and therefore it can protect the nozzle wall from the hot main flow more efficiently.

Film cooling efficiency can be predicted by various ways. The simplest one is to use experimental data correlations. However, the range of applicability of these correlations is limited and often unknown; therefore they are not reliable. On the other hand, although computational fluid dynamics (CFD) can be used to solve boundary-layer or Navier–Stokes equations, a first comparison between CFD results and correlations shows a large scatter in the predictions of the distance over which the film fully protects the wall as well as in the computed wall temperature at the nozzle exit.

There exists a large amount of experimental data on supersonic film cooling in the literature,[2–12] which cover a wide range of external and film Mach numbers and show that film cooling is much more efficient in supersonic flows than in subsonic flows. Unfortunately, the existing literature could not be used to validate a numerical approach for application to the Vulcain engine. First of all, no test case was close to the engine conditions in terms of the similarity parameters defined in Sec. II.A. Nethertheless, some of these data were used as preliminary tests to validate the numerical approach. But, due to the lack of data on inflow conditions, on the development of the velocity and temperature profiles downstream of the injector, and on the wall temperature and heat exchanges coefficient evolution, it was very difficult to validate the numerical approach. Therefore, it was decided to conduct a new experimental study on film cooling with an aim to validate the numerical tools.

II. Experimental Study

A. Similarity

In the Vulcain engine, the film is produced by the injection of the turbine exhaust gases. The exhaust gases are first collected in a torus and then injected in the engine nozzle through a short nozzle. The film is a supersonic film with a large inviscid core. The mixing of the film with the main flow occurs first through a mixing layer and eventually merges with the wall boundary layer. It was thus important to try to reproduce the key parameters of the mixing layer. These key parameters are the Mach numbers of the film and of the main flow, a Reynolds number based on the injection height, the ratio between the film and main mass flows $\lambda = (\rho U)_f/(\rho U)_m$, the convective Mach number $M_c = (U_m - U_f)/(a_m + a_f)$, and

Received Dec. 1, 1995; presented as Paper 96-0657 at the AIAA 34th Aerospace Sciences Meeting, Reno, NV, Jan. 15–18, 1996; revision received Oct. 30, 1997; accepted for publication Jan. 9, 1998.

*Head of Research Unit, Turbulence, Modelling, and Prediction, Department of Modelling in Aerodynamics and Energetics, B.P. 4025, 2, Avenue E. Belin. E-mail: Bertrand.Aupoix@onecert.fr.

†Head of Research Unit, Experimental Methods and Techniques, Department of Modelling in Aerodynamics and Energetics, B.P. 4025, 2, Avenue E. Belin.

‡Ph.D. Student, Department of Modelling in Aerodynamics and Energetics; currently Engineer, Aerospatiale, 316, Route de Bayonne, 31060 Toulouse Cedex 03, France.

§Research Engineer, Fundamental and Experimental Aerodynamics Department, 8, rue des Vertugadins.

the temperature or density ratio of the two flows. Although the mixing-layer development is too short a distance to reach a self-similarity state, the convective Mach number and the density ratio were selected as the major parameters because they strongly affect the mixing-layer spreading rate.[13]

In the engine, the main flow is mainly high temperature water vapor, and the film is a hydrogen-rich hydrogen/water vapor mixture at a lower temperature. To provide a convenient way to investigate the flow structure, standard gases at moderate temperatures were preferred for the experimental study. The use of a conventional wind tunnel was selected. A cryogenic technology was chosen to obtain a cold film containing a mixture of air and vaporized liquid nitrogen. Therefore, it was impossible to reproduce all the similarity parameters. The main flow Mach number and the convective Mach number, which were selected as the key parameters, were duplicated. The lower temperature ratio was sought, but the temperature and density ratios, as well as the isentropic exponent of the gases, the film Mach number, and the mass flow ratio λ, were not duplicated. The injection Reynolds number was duplicated only during the first test stage.

B. Experimental Setup

The experimental setup was first validated with two correlations due to Trolier (cited in Ref. 14) and a boundary-layer computation using Chien's k–ε model. The objective was to check if the film would break in the measurement zone. These three approaches previously gave similar results for the engine case. When applied to the experiment, only one correlation was in agreement with the boundary-layer computation, whereas the other one predicted a film protection length three times smaller. This illustrates the large uncertainty associated with the use of correlations.

The experiments were conducted in the ONERA S5Ch wind tunnel in Chalais–Meudon. This is a continuous facility running with desiccated air. The experiment time of about 30 min was just limited by the liquid nitrogen storage for the cold film. The supersonic nozzle was set in a half-nozzle configuration, i.e., the lower wall was contoured, but the upper wall, along which experiments were conducted, was flat.

To facilitate the comparison between computations and experiments, a two-dimensional geometry was designed. A sketch of the model is shown in Fig. 1, where viscous regions are shaded. The measurement plate is located in the constant Mach number region of the wind tunnel.

The test section is 154 mm high and 289 mm wide, and the constant Mach number region is 450 mm long. In this configuration, the Mach number is 2.78 in the constant Mach number region of the test section. The stagnation pressure and temperature of the main flow are 800 mbar and 320 K. The static pressure and temperature in the test section are thus about 30 mbar and 125 K.

The cryogenic film was generated by vaporizing liquid nitrogen into air in a mixing chamber. Then the flow passes through an insulated settling chamber before being injected through a short nozzle that has been designed to give a film Mach number close to 2. The minimum stagnation temperature for the film was initially designed to be 108 K but had to be increased to 125 K to avoid rime on the measurement plate. This corresponds to a static temperature of about 70 K and a convective Mach number of 0.73, close to engine operating conditions. The ratio of the film and main flow temperatures was larger than that for the engine.

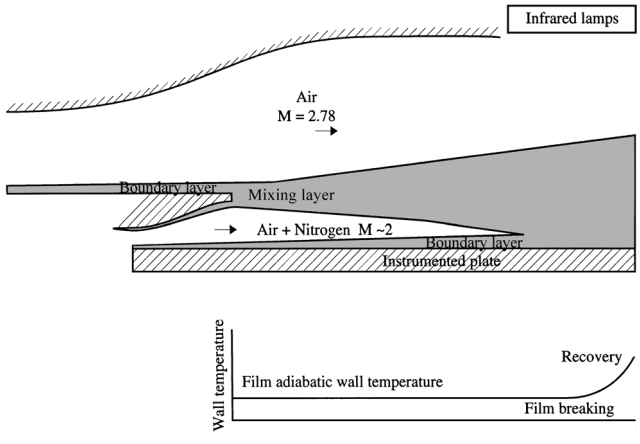

Fig. 1 Sketch of the film-cooling experiment.

A film at ambient temperature was also investigated to study the influence of the film temperature, which is known to strongly affect the mixing-layer spreading rate. This influence is caused by the density and velocity ratios as well as the convective Mach numbers being modified. The stagnation and static temperatures were 260 and 144 K, respectively. The convective Mach number was reduced to 0.24.

The liquid nitrogen mass flow was monitored to achieve the required film temperature. At the same time, the film pressure was also monitored. The focus was first on adapted (or matched) flow conditions, i.e., when the static pressures of both flows are equal. Nevertheless, the mixing chamber control device was designed to investigate the influence of the pressure mismatch. Pressure mismatches of about $\pm 50\%$ were achieved to reproduce flow conditions that could be encountered on the engine.

Two measurement trials were performed. In the first one, the film injector was a symmetrical nozzle, with an exit height of 10.5 mm to duplicate the engine Reynolds number (and, fortuitously, the engine injector height). The mixing-layer development was well documented, but the film did not break in the test section. Moreover, thermal leaks were identified in this trial so that the experimental setup had to be modified.

Therefore, a second experimental trial with a half-nozzle configuration for the injector (as shown in Fig. 1) and an injector height of about 5.6 mm was used to investigate the film breaking. Because of the low static pressure, the Reynolds number of the boundary layer at the injector nozzle exit was very low. Wires were installed in the convergent part of the injector nozzle to trigger the boundary layer. Formation of rime cones downstream from small roughnesses in cold film flows and boundary-layer probings show that the boundary layer was still laminar. Small three-dimensional roughnesses were installed to force transition at the injector exit. No rime formation and boundary-layer surveys proved that the boundary layer was then fully turbulent. In both experiments, the lip thickness was 0.9 mm.

C. Measurement Techniques

Schlieren visualizations were used to monitor the flow and to show the variations of flow structure when the film pressure or temperature is changed. For the first trial, strioscopic glass was used for the side wall windows, but this required two side films at room temperature to avoid thermal cracks of the glass. In the second trial, these side films, which caused thermal problems, were removed and Plexiglas® windows were used.

A few pressure taps and thermocouples are placed in the wind-tunnel symmetry axis upstream of the film injection to monitor the incoming flow conditions.

The measurement plate is made of Isotan, a nickel/copper alloy, and is 7 mm thick. Thermal leaks were evidenced in the first test trial, and therefore the plate was insulated in the second trial. The wind-tunnel running time is long enough to reach a thermal steady state. The longitudinal distributions of wall pressure and temperature are measured in two lines close to the symmetry axis with 18 pressure taps and 18 thermocouples, at a constant spacing of 25 mm. Two extra transverse rows of pressure taps and thermocouples are used to check the two-dimensional character of the flow.

Passive thermography[15] was used to determine the heat transfer coefficients. A set of 12 infrared lamps of 2000-W power each was installed in the facility in front of the plate and outside of the flow, as shown in Fig. 1. A water-cooled, quick aperture shutter in front of these lamps enables a quick start and stop of the plate illumination so as to generate a heat pulse during 7 s. The plate has been coated with a black paint to absorb radiation. The time evolution of the surface temperature is measured by the thermocouples. The analysis of the temperature relaxation after the heat pulse gives access to the heat transfer coefficients.

Boundary-layer measurements were performed with a three-probe rake. Static and stagnation pressures, together with stagnation

temperature, were recorded simultaneously. The static pressure probe allows one to document the static pressure variations through the boundary layer near the lip where boundary-layer assumptions fail. Because pressure measurements only yield the Mach number values, the stagnation temperature probe permits one to deduce the velocity and hence to investigate the thermal mixing. The temperature probe was located farther from the wall than the pressure probes to protect it. All of the temperature measurements have thus been interpolated to the same wall distance as pressure measurements during the data reduction process.

Pressure was measured with an accuracy better than ± 0.5 mbar over the pressure range (80–800 mbar) and temperatures with ± 1.5 K over the temperature range (120–320 K). Probe locations were known with an 0.1-mm accuracy along the wall normal and 0.5-mm accuracy in the other two directions.

D. Key Experimental Results

1. Flow Two-Dimensionality

The two-dimensional character of the flow was systematically checked using wall pressure and temperature measurements in the transverse direction along different wall distances. In the first trial, thermal leaks and thermal disturbances due to the side films were important, and therefore the wall temperature presented significant spanwise variations, with a plateau near the symmetry axis. All other measured quantities showed a good two-dimensional character.

2. Schlieren Flow Visualizations

Two schlieren visualizations for the 10.5-mm injector configuration are given in Figs. 2 and 3 for an underexpanded film ($p_f/p_m = 1.5$) and an overexpanded film ($p_f/p_m = 0.75$), respectively. In the experiment, the plate is indeed above the flow, in contrast to Fig. 1 and computational results. Because the lip thickness is not small compared with the boundary-layer thickness, the forming of the mixing layer as a result of the merging of the main flow and the injector boundary layers occurs, and it causes a shrinking of the viscous region downstream from the lip. The inviscid flow must also deviate; the two so-formed expansion waves (a), which originate from the lip edges, are clearly visible. The point (b), where the expansion wave originating from the lip strikes the wall, moves downstream as the film pressure increases. The mixing layer (c) is also clearly visible. It moves farther from the wall as the film pressure increases. At last, another expansion wave (d) starts at the beginning of the plate. It is due to a step caused by a Teflon® seal that was removed in the second trial.

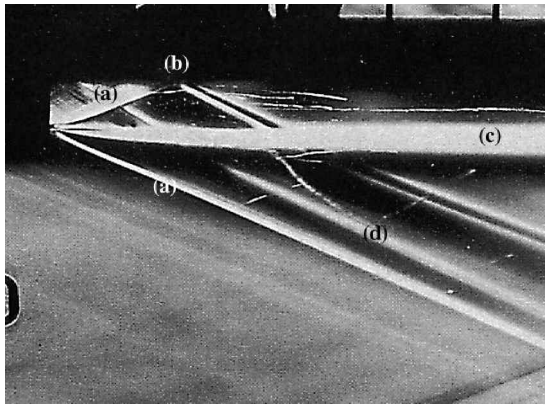

Fig. 2 Schlieren visualization of an underexpanded film.

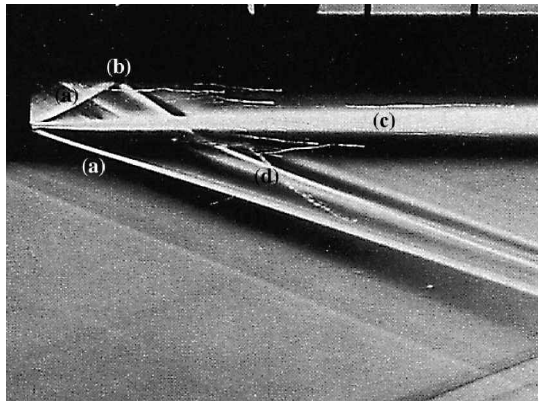

Fig. 3 Schlieren visualization of an overexpanded film.

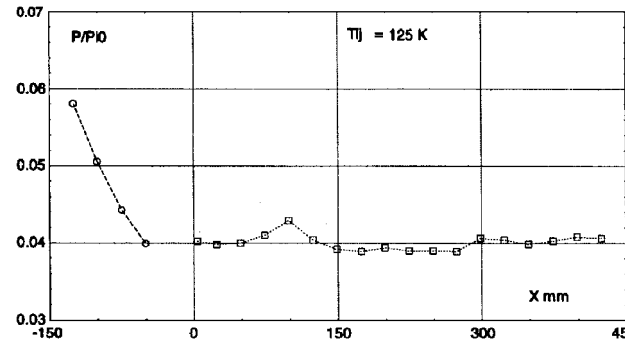

Fig. 4 Wall pressure measurement: injector height 5.6 mm, cold film, matched conditions.

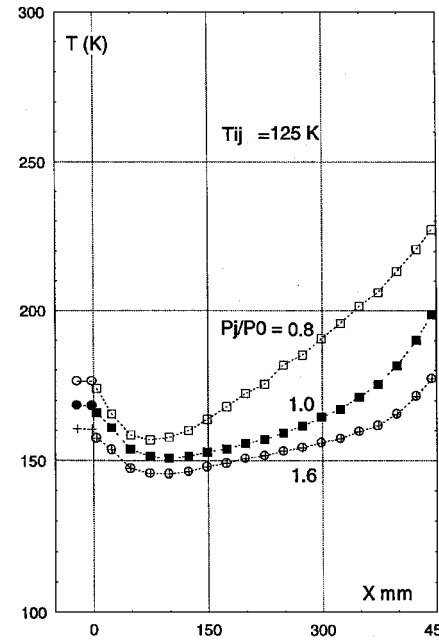

Fig. 5 Influence of the film pressure on the wall temperature evolution: injector height 5.6 mm, cold film.

3. Wall Pressure Distribution

Without the film injector, the wall pressure should be constant. The existence of the film and the expansion waves at the injector lip slightly alter this situation, as shown in Fig. 4. The origin of the axis is at the injector, and the pressure decrease upstream from the injector corresponds to the wall pressure evolution in the wind-tunnel nozzle.

4. Wall Temperature Distribution

The wall temperature distribution is plotted in Fig. 5, where the results for a cold film with the small injector are displayed. Some thermal leaks are still present as the adiabatic temperature of 119 K is not retrieved. No temperature plateau can thus be observed. However, the trends are clear: as the film pressure is increased, the film better cools the wall and protects it on a longer distance.

Because the static pressure is low, the heat transfer coefficients are also small, with an average value of about 100 $\mathrm{Wm^{-2}\,K^{-1}}$. They are difficult to measure as the heating is not uniform along the plate due to the rearward location of the set of infrared lamps.

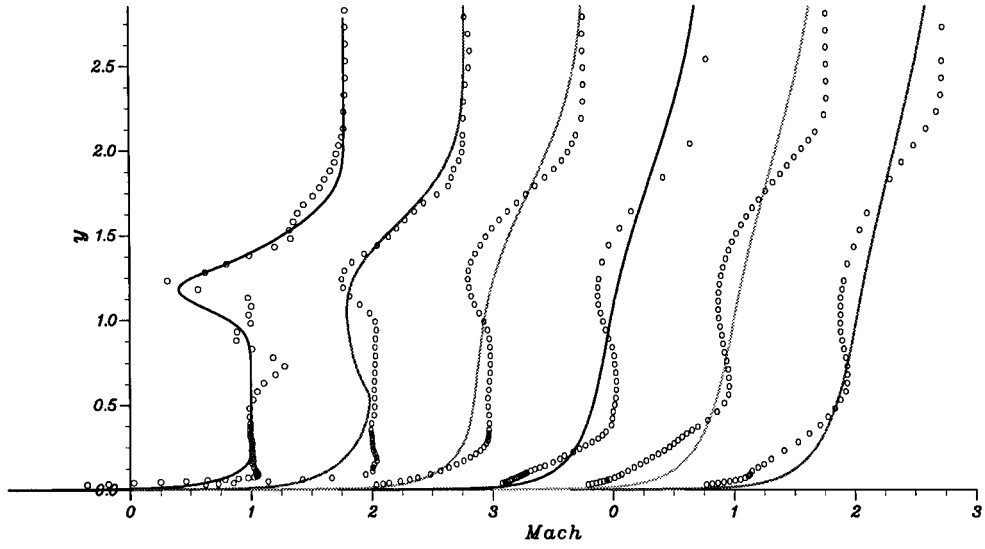

Fig. 6 Mach number profiles: injector height 10.5 mm, cold film, model of Baldwin and Lomax.[23]

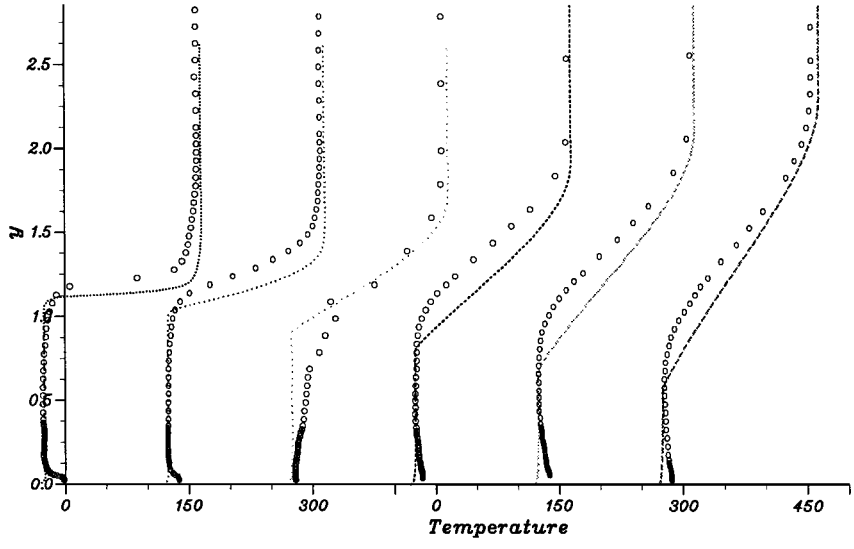

Fig. 7 Stagnation temperature profiles: injector height 10.5 mm, cold film, model of Jones and Launder.[24]

5. Mean Flow Profiles

Measured Mach number and stagnation temperature profiles are given for the cold and adapted film, high injector case in Figs. 6 and 7, respectively. The wall distance y is in centimeters; experimental profiles are plotted with symbols for stations 0.01, 0.055, 0.132, 0.20, 0.27, and 0.34 m downstream from the injector lip. The kink on the first profile is due to the expansion wave originating from the lip. An inviscid core initially fills the region between the wall boundary layer and the mixing layer. Its progressive thinning as the mixing layer spreads is clearly visible. The expansion of the mixing layer and the recovery toward an equilibrium boundary layer are slow.

III. Computational Study

A. Use of a Boundary-Layer Approach

Various approaches have been used to compute film cooling in supersonic flows, ranging from boundary-layer approaches[16] to parabolized and Navier–Stokes approaches.[17–19] Of course, a boundary-layer approach is a priori restricted to matched conditions. Moreover, it is not adequate near the injector lip as the streamwise gradients are comparable to the gradients along the wall normal direction, and therefore there exists a normal pressure gradient in the mixing layer. On the other hand, it is inexpensive compared with the Navier–Stokes approaches. Therefore, the goal of this investigation was twofold: to check the ability of a boundary-layer approach to compute such flows and to compare the predictions of various turbulence models.

The code[20,21] solves compressible boundary-layer equations, using a finite volume technique, a self-adaptive grid along the wall normal, and the space-marching directions. The grid along the wall normal is adapted, when necessary, according to the first- and second-order derivatives of the velocity, enthalpy, and turbulent quantities profiles. Several levels of grid refinement can be selected. The marching step is determined by the code, according to the variation of the boundary-layer profiles between two stations. Here again, several refinement levels are available.

Special attention must be paid to treat the singularity that exists in the boundary-layer equations at the injector lip. A very small marching step had to be chosen just downstream from the injector, and the marching step of course was automatically increased by the code farther downstream. Similarly, a fine grid resolution with more than 200 points along the wall normal was required. It has been checked that the results were independent of the grid; i.e., identical results were achieved with finer grids, both along the wall normal and in the marching direction. Nevertheless, the cost of a boundary-layer computation was still negligible compared with that for the full Navier–Stokes equations.

The computation procedure is as follows. First, inviscid solutions in the wind tunnel and injector nozzles are obtained with a method of characteristics. Then, the boundary layers that develop along the

wind-tunnel walls and in the injector are computed by the boundary-layer code with boundary conditions provided by the inviscid solutions. At the injector lip, all these solutions have to be assembled to generate a new initial profile. Starting from the wall, there are first the injector wall boundary layer, the injector inviscid flow core, the injector boundary layer on the lip, the "lip flow," and then the main flow boundary layer (see Fig. 1). This profile is thus the initial profile for a new boundary-layer computation of the mixing zone downstream from the injector. All boundary-layer computations assume a steady regime, i.e., adiabatic wall conditions.

The lip flow means that the velocity or the turbulent kinetic energy are zero at the lip, but to avoid a singularity in the boundary-layer equations and to start the space-marching procedure, they have to be set at very small but nonzero values. It has been checked that the results are not sensitive to the chosen values.

B. Turbulence Models

A large variety of eddy viscosity turbulence models have been tested. The Cebeci and Smith[22] and the Baldwin and Lomax[23] algebraic models have been investigated because they are very simple and inexpensive.

Two equation models, of the $k-\varepsilon$ and the $k-\omega$ types, are more relevant to this kind of flow situation where the turbulence is far from equilibrium and the turbulence length scale cannot be simply related to the flow geometry. Five $k-\varepsilon$ models due, respectively, to Jones and Launder,[24] Launder and Sharma,[25] Chien,[26] Nagano and Tagawa,[27] and So et al.[28] have been tested. The first two are very similar. Chien's model mainly differs from Launder's models by the use of the wall distance instead of the turbulent Reynolds number in the wall damping functions, which may affect the prediction of the mixing layer and the early stages of the mixing layer merging with the boundary layer. All three models solve an equation for a pseudodissipation that is zero at the wall. The last two models solve a transport equation for the unmodified dissipation. The model of So et al. differs by the use of unusual diffusion coefficients in the transport equations. The $k-\omega$ model used here is due to Wilcox.[30]

Finally, a four-equation model due to Sommer et al.,[29] which is an extension of the So et al.[28] $k-e$ model with two extra equations for the temperature fluctuation variance and its associated dissipation rate, has been tested. The goal was to get rid of the assumption of a constant turbulent Prandtl number to compute the turbulent heat fluxes as experiments tend to show that the turbulent Prandtl number is roughly constant in boundary layers and in mixing layers but with different levels.

Moreover, it is well known that most of the turbulence models are unable to correctly predict the reduction of the mixing-layer spreading rate as the convective Mach number increases. This is usually blamed on the compressible character of the turbulent motion. Various modifications have been proposed in the literature. We tested several exploratory models but will discuss here only the compressibility correction of Sarkar[31] for the dilatational dissipation. This modification was implemented in Chien's[26] $k-\varepsilon$ model.

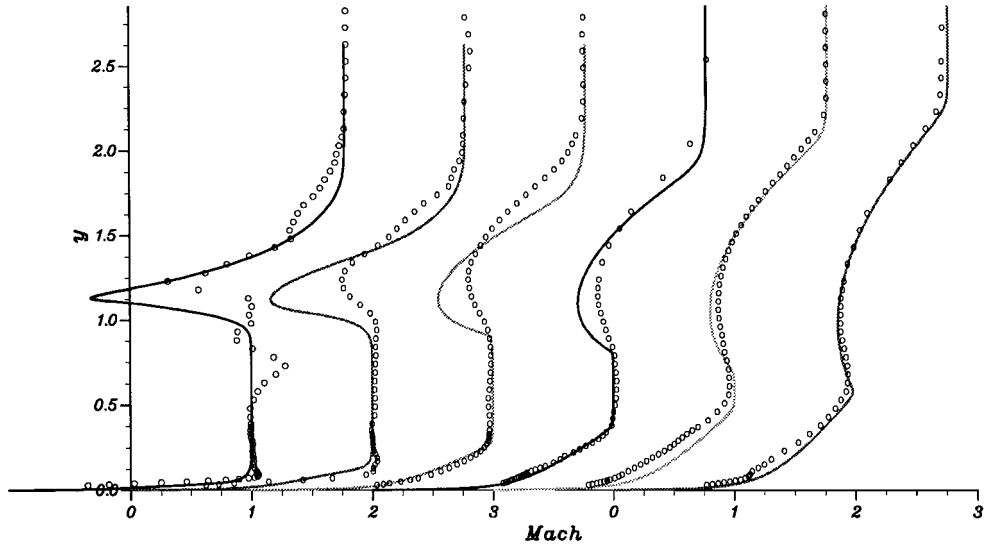

Fig. 8 Mach number profiles: injector height 10.5 mm, cold film, model of Jones and Launder.[24]

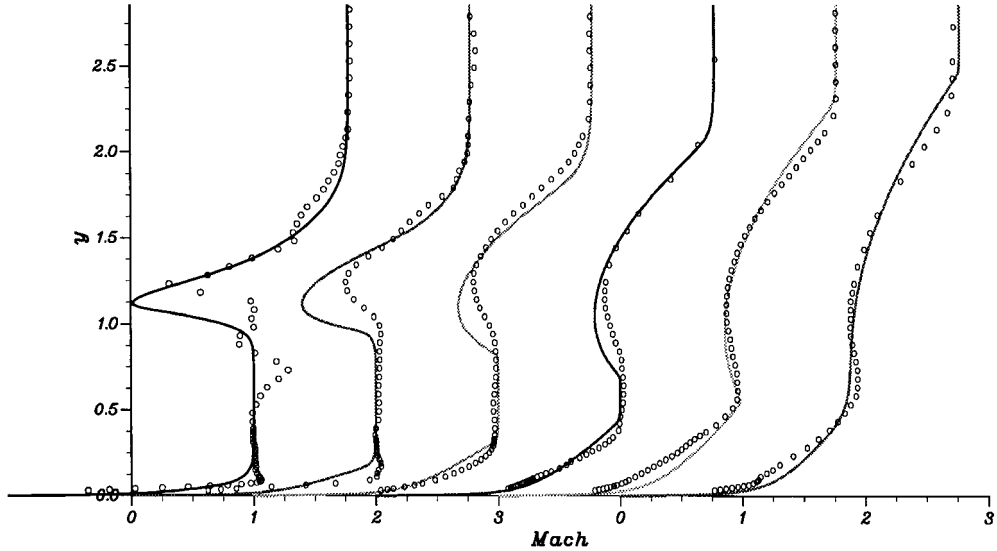

Fig. 9 Mach number profiles: injector height 10.5 mm, cold film, model of Chien.[26]

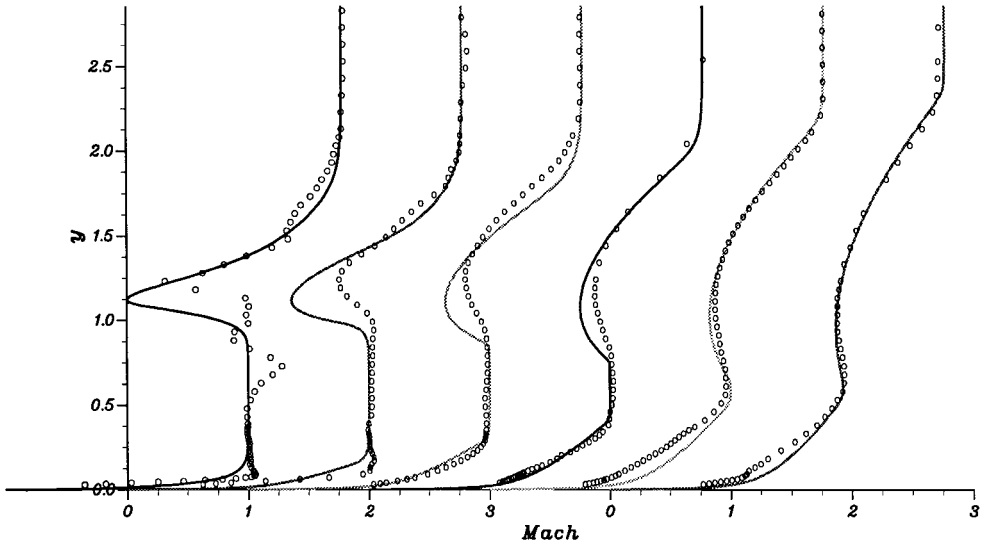

Fig. 10 Mach number profiles: injector height 10.5 mm, cold film, Chien's[26] model with Sarkar's[31] compressibility correction.

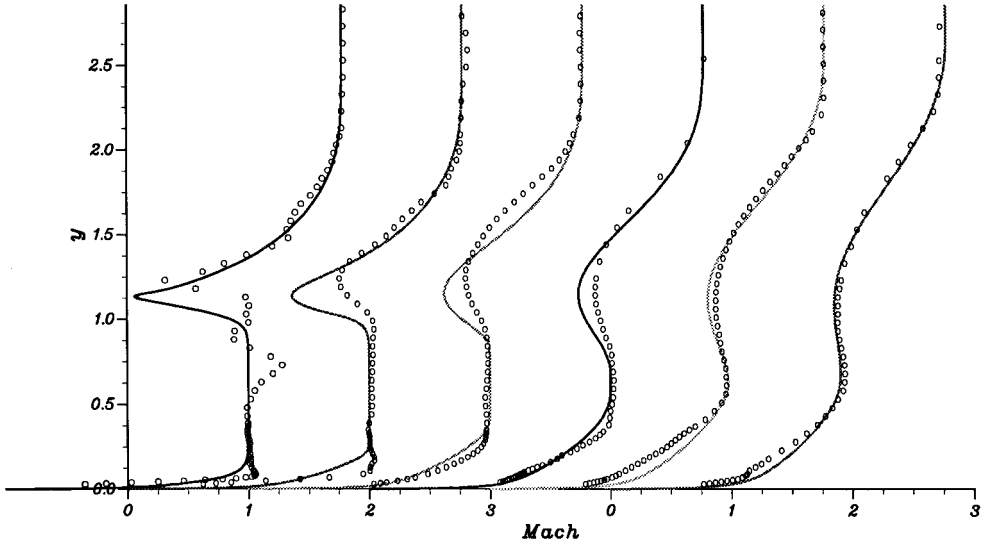

Fig. 11 Mach number profiles: injector height 10.5 mm, cold film, model of So et al.[28]

C. Comparisons Between Boundary-Layer Computations and Experiments

The four cases of matched film, i.e., for the two injector heights and the two film temperatures, have been investigated.

The results for the higher injector case will be presented first because they give more information about the development of the mixing layer. The emphasis is put on the cold film case because the convective Mach number is large. In Figs. 6–11, the wall distance y is in centimeters and experimental (symbols) and computed (lines) profiles are compared for stations 0.01, 0.055, 0.132, 0.20, 0.27, and 0.34 m downstream from the injector lip.

Algebraic models' predictions are very poor. These models only deal with global information on the turbulence length scale deduced from the flow geometry. The models assume that the wall boundary layer and the mixing layer are essentially the same layer, even before they have merged, and that the thickness of this layer gives the turbulence length scale. The models overestimate the turbulence length scale and the turbulent diffusion, and therefore they predict a very rapid mixing and a very quick relaxation toward an equilibrium boundary-layer solution (Fig. 6).

Predictions of the Jones and Launder[24] k–ε model are given in Figs. 7 and 8 for the higher-injector, cold film configuration. It can first be noted that the agreement on the Mach number profiles is fair for the last stations, whereas there is a visible shift between the experimental and computed temperature profiles. If only pressures had been measured, only the Mach number profiles would have been available, and the computations would have appeared in agreement with the experiments. This shows the importance of measuring not only the stagnation pressure but also the stagnation temperature to have access to more information about the flowfield. Errors on the velocity and temperature profiles here roughly compensate to give a good prediction of the Mach number profile.

The shift between the experimental and computed temperature profiles can be explained by the use of the boundary-layer equations. They cannot account for the normal pressure gradient near the lip nor for the presence of expansion waves. Moreover, as streamwise diffusion is neglected, streamwise gradients are overestimated. Through the continuity equation, an error on the streamwise gradient of the longitudinal velocity component yields an underestimation of the wall normal velocity component and a downwash of the computed profiles. The shortcomings of the boundary-layer assumptions may also be the cause of a poor prediction of the wake of the injector lip at the stations downstream from the injector. Exploratory Navier–Stokes computations performed at ONERA Chatillon by C. Notin and L. Cambier have shown that such an approach better reproduces the value and location of the minimum Mach number value in the lip wake. At last, it can be noted that the mixing-layer expansion rate is overestimated by the Jones and Launder k–ε model, as expected.

Predictions of the Chien[26] k–ε model, without and with compressibility correction, are given in Figs. 9 and 10, respectively.

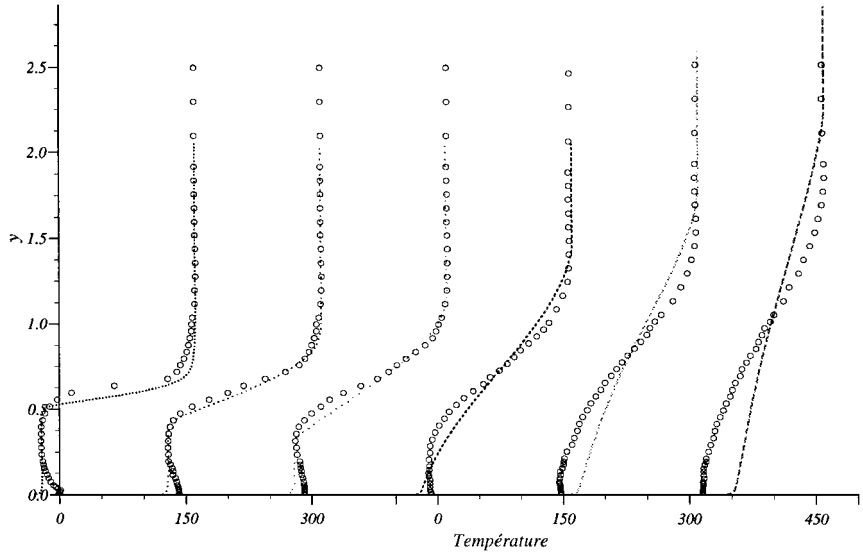

Fig. 12 Temperature profiles: injector height 5.6 mm, cold film, model of Chien.[26]

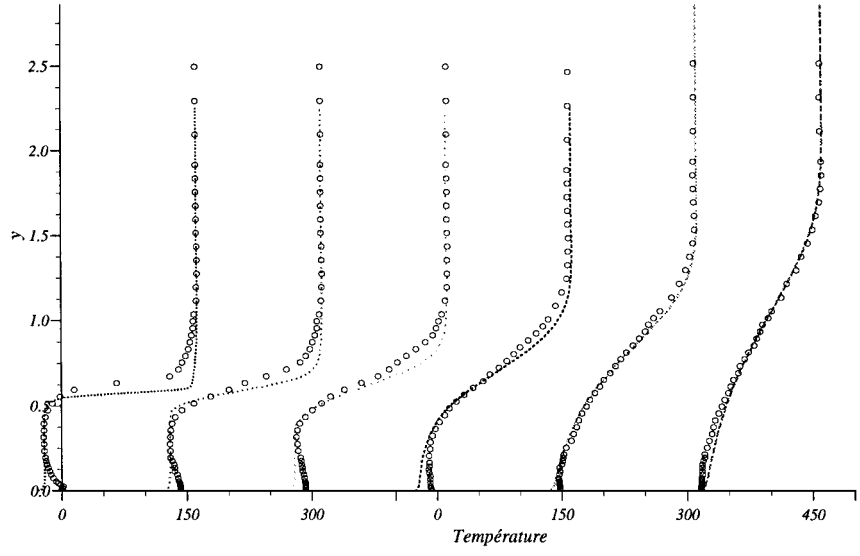

Fig. 13 Temperature profiles: injector height 5.6 mm, cold film, model of So et al.[28]

Chien's model also strongly overestimates the mixing-layer spreading rate. Sarkar's compressibility correction[31] reduces the mixing-layer spreading rate and thus improves the prediction.

The best predictions are achieved with the So et al.[28] model, as shown in Fig. 11. This model fairly reproduces the mixing-layer spreading rate. Because there is no compressible turbulence correction in this model, this seems to be due to the use of unusual diffusion coefficients in the turbulence transport equations, which allows a better prediction of the outer region of the mixing layer. The use of extra equations to compute the turbulent Prandtl number did not improve the results. The Sommer et al.[29] model is unable to predict the turbulent Prandtl number in the mixing layer.

The Wilcox[30] k–ω model predicts a mixing-layer expansion rate similar to Chien's model.

The lower convective Mach number in the ambient temperature case reduces the differences between the models' predictions.

For the higher injector case, the film may break by the end of the plate, but due to uncontrollable thermal leaks at the end of the plate, the exact breaking point could not be determined. However, computations showed a very significant change between the cold and ambient temperature film cases. For the cold film cases, k–ε models predict a breaking point between 0.3 and 0.4 m downstream from the injector. For the ambient temperature film case, no breaking was predicted in the computed domain, which extends down to 0.5 m from the injector. Because the film Mach number and the static pressure are fixed, $u_f \sim \sqrt{T_f}$, whereas $\rho_f \sim T_f^{-1}$. Therefore, the mass flow

$$\rho_f u_f \sim T_f^{-\frac{1}{2}}$$

is lower for the ambient film flow, and it is surprising that a hotter film protects better. Moreover, the convective Mach number is also lower. Let us remember that the mixing-layer expansion rate reads

$$\delta' = \delta'_{\text{inc}} F(M_c)$$

where δ'_{inc} is the expansion rate in incompressible flows and F is a decreasing function. It is expected that a decrease in the convective Mach number yields an increase of the expansion rate. In fact, the expansion rate is here governed by the change in the density ratio. Papamoschou and Roshko[13] give the following relation for the expansion rate in incompressible flows:

$$\delta'_{\text{inc}} = \frac{[1 - (u_m/u_f)]\left(1 + \sqrt{\rho_m/\rho_f}\right)}{1 + (u_m/u_f)\sqrt{\rho_m/\rho_f}}$$

Because of the temperature dependency of the velocity and the density, the incompressible expansion rate is three times bigger in the case of the cold film compared with the ambient temperature film. This explains why the cold film is less efficient than the ambient

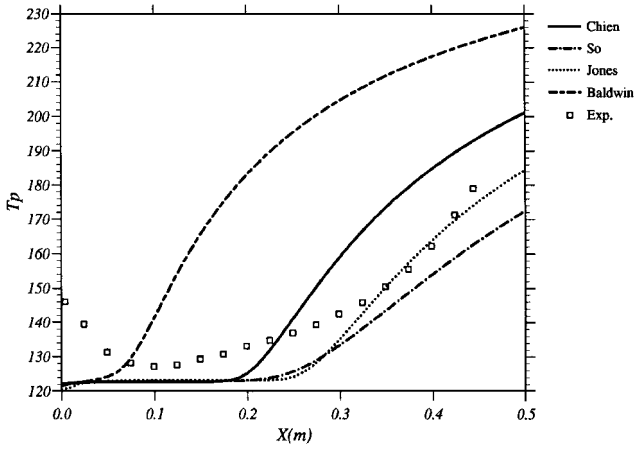

Fig. 14 Adiabatic wall temperature evolution: injector height 5.6 mm, cold film.

temperature film and also shows that the mass flow ratio λ, although often used, is not always the relevant parameter to correlate supersonic film cooling efficiencies.

The smaller injector height case provides data on the film breaking and the relaxation toward an equilibrium boundary layer. Moreover, data on the wall temperature evolution are available.

This case shows that a good prediction of the mixing layer, before it merges with the wall boundary layer and diffuses down to the wall, is required to correctly predict the relaxation of the boundary layer toward an equilibrium state downstream from the film breaking. Here again, the best results are achieved with the So et al. model, as shown in Figs. 12 and 13. The wall distance y is still in centimeters, and the profiles are compared at stations 0.01, 0.049, 0.19, 0.20, 0.30, and 0.448 m downstream from the injector lip. The prediction of the adiabatic wall temperature shows that transport equation models can fairly reproduce the film-breaking location and the temperature increase downstream, whereas algebraic models predict a too early film breaking (Fig. 14). Some thermal leaks in the experiment are visible in this figure because there is no plateau on the measured adiabatic wall temperatures. The film however, protects for at least 0.3 m before breaking. The Jones and Launder and So et al. models yield the best predictions of the fully protected length and of the wall temperature recovery. The wall temperature data have been approximately corrected to account for the thermal leaks by estimating the increase of the wall temperature due to thermal leaks upstream of the film-breaking point and subtracting this drift to the measured wall temperature. The model of So et al.[28] then gives the best prediction of the temperature recovery downstream from the film breaking. Heat transfer coefficient predictions are in good agreement with measurements. At last, computations show a decrease of the skin friction downstream from the injection.

IV. Conclusions

Film cooling has been investigated for two geometries, two film temperatures, and three pressure ratios. This gives a large database to validate numerical approaches and turbulence models. Schlierens give a comprehensive survey of the flow structure, whereas wall measurements as well as flow probings down to the wall permit a complete description of the mixing process.

This experiment shows why film cooling is much more efficient in supersonic than in subsonic flows. First of all, a supersonic film has to be expanded through a nozzle so that the film is an inviscid core with thin boundary layers. The turbulent length scales in the film are small, and the mixing is reduced. Moreover, the spreading rate of the so-formed mixing layer can be controlled, via the velocity and density ratios and the convective Mach number, to further reduce the mixing.

Although a boundary-layer approach is not correct near the injector lip and thus predicts a small downwash of the mixing layer, it is a very efficient and inexpensive way to investigate film cooling. Algebraic models are not well suited to predict such flows, whereas two-equation models correctly reproduce the key features of the flow. A good prediction of the mixing layer is required to fairly reproduce all the details of the flow. Among the tested models, the So et al. model seems to be the best.

Acknowledgments

It is the authors' pleasure to acknowledge the Centre National d'Études Spatiales, which granted this research together with the Société Européenne de Propulsion, DASA, and Volvo for their fruitful contributions to this work. The experimental study could not have been performed without the contribution of H. Consigny, C. Pérouze, G. Rancarani, C. Rigoulet, and N. Séverac. The important contribution of K. Talarek, the advice of J. Schetz, and the final review of the manuscript by G. Huang were highly appreciated.

References

[1] Vuillermoz, P., Weiland, C., Aupoix, B., Grosdemange, H., and Bigert, M., "Advanced Nozzle Technology for Cryogenic Engines," *Second International Symposium on Liquid Rocket Propulsion*, ONERA, Chatillon, France, 1995, pp. 23-1–23-20.

[2] Visich, M., Jr., and Libby, P. A., "Experimental Investigation of Mixing of Mach Number 3.95 Stream in Presence of Walls," NACA TN D-247, Feb. 1960.

[3] Goldstein, R. J., Eckert, E. R. G., Tsou, F. K., and Haji-Sheikh, A., "Film Cooling with Air and Helium Injection Through a Rearward-Facing Slot into a Supersonic Air Flow," *AIAA Journal*, Vol. 4, No. 6, 1966, pp. 981–985.

[4] Zakkay, V., Sakell, L., and Parthasarathy, K., "An Experimental Investigation of Supersonic Slot Cooling," *Heat Transfer and Fluid Mechanics Conference*, Stanford Univ. Press, Stanford, CA, 1970, pp. 88–103.

[5] Cary, A. M., Jr., and Hefner, J. N., "Film-Cooling Effectiveness and Skin Friction in Hypersonic Turbulent Flows," *AIAA Journal*, Vol. 10, No. 9, 1972, pp. 1188–1193.

[6] Zakkay, V., Wang, C. R., and Miyazawa, M., "Effect of Adverse Pressure Gradient on Film Cooling Effectiveness," *AIAA Journal*, Vol. 12, No. 5, 1974, pp. 708, 709.

[7] Bass, R. W., Hardin, L. W., Rodgers, R. J., and Ernst, R. C., "Supersonic Film Cooling," AIAA Paper 90-5239, 1990.

[8] Hyde, C. R., Smith, B. R., Schetz, J. A., and Walker, D. A., "Turbulence Measurements for Heated Gas Slot Injection in Supersonic Flow," *AIAA Journal*, Vol. 28, No. 9, 1990, pp. 1605–1614.

[9] Olsen, G. C., Nowak, R. N., Holden, M. S., and Baker, N. R., "Experimental Results for Film Cooling in 2-D Supersonic Flow Including Coolant Delivery Pressure, Geometry, and Incident Shock Effects," AIAA Paper 90-0605, Jan. 1990.

[10] Hansmann, T., and Wilhelmi, H., "An Experimental Investigation of the Film-Cooling Process at High Temperatures and Velocities," AIAA Paper 93-5062, Dec. 1993.

[11] Stafford, M. A., and Hartfield, R. J., Jr., "Experimental Investigation of Slot Injection into Supersonic Flow with an Adverse Pressure Gradient," AIAA Paper 93-2442, June 1993.

[12] Juhany, K. A., Hunt, M. L., and Sivo, J. M., "Influence of Injectant Mach Number and Temperature on Supersonic Film Cooling," *Journal of Thermophysics and Heat Transfer*, Vol. 8, No. 1, 1994, pp. 59–67.

[13] Papamoschou, D., and Roshko, A., "The Compressible Turbulent Shear Layer: An Experimental Study," *Journal of Fluid Mechanics*, Vol. 197, Dec. 1988, pp. 453–477.

[14] Majeski, J. A., and Weatherford, R. H., "Development of an Empirical Correlation for Film-Cooling Effectiveness," AIAA Paper 88-2624, June 1988.

[15] Balageas, D. L., Boscher, D. M., Déom, A. A., Fournier, J., and Gardette, G., "Application de la thermographie infrarouge passive et stimulée à la mesure des flux thermiques en soufflerie," *La Recherche Aérospatiale*, Vol. 4, July–Aug. 1991, pp. 51–72.

[16] Beckwith, I. E., and Bushnell, D. M., "Calculation by a Finite-Difference Method of Supersonic Turbulent Boundary Layers with Tangential Slot Injection," NASA TN-D-6221, April 1971.

[17] Wang, J., "Prediction of Turbulent Mixing and Film-Cooling Effectiveness for Hypersonic Flows," AIAA Paper 89-1867, June 1989.

[18] O'Connor, J. P., and Haji-Sheikh, A., "Numerical Study of Film Cooling in Supersonic Flow," *AIAA Journal*, Vol. 30, No. 10, 1992, pp. 2426–2433.

[19] Kacynski, K. J., and Hoffman, D., "The Prediction of Nozzle Performance and Heat Transfer in Hydrogen/Oxygen Rocket Engines with Transpiration Cooling, Film Cooling and High Area Ratios," AIAA Paper 94-2757, June 1994.

[20] Aupoix, B., "Calcul des couches limites compressibles bidimensionnelles. Programmes CLIC et EQUI," ONERA, Rapport Technique OA 42/5005.42, July 1991.

[21] Aupoix, B., and Arnal, D., "CLIC: Calcul des couches limites compressibles," ONERA, Rapport Technique OA 23/5005.09 AYD, Oct. 1988.

[22] Cebeci, T., and Smith, A. M. O., "Analysis of Turbulent Boundary Layers," *Applied Mathematics and Mechanics*, Vol. 15, Academic, 1974.

[23]Baldwin, B. S., and Lomax, H., "Thin Layer Approximation and Algebraic Model for Separated Turbulent Flows," AIAA Paper 78-257, Jan. 1978.

[24]Jones, W. P., and Launder, B. E., "The Prediction of Laminarization with a Two-Equation Model of Turbulence," *International Journal of Heat and Mass Transfer*, Vol. 15, Feb. 1972, pp. 301–314.

[25]Launder, B. E., and Sharma, B. I., "Application of Energy-Dissipation Model of Turbulence to the Calculation of Flow Near a Spinning Disc," *Letters in Heat and Mass Transfer*, Vol. 1, 1974, pp. 131–138.

[26]Chien, K. Y., "Predictions of Channel and Boundary-Layer Flows with a Low-Reynolds-Number Turbulence Model," *AIAA Journal*, Vol. 20, No. 1, 1982, pp. 33–38.

[27]Nagano, Y., and Tagawa, M., "An Improved k–ε Model for Boundary Layer Flows," *Journal of Fluids Engineering*, Vol. 112, March 1990, pp. 33–39.

[28]So, R. M. C., Zhang, H. S., and Speziale, C. G., "Near-Wall Modeling of the Dissipation-Rate Equation," AIAA Paper 92-0441, Jan. 1992.

[29]Sommer, T. P., So, R. M. C., and Zhang, H. S., "Near-Wall Variable Prandtl-Number Turbulence Model for Compressible Flows," *AIAA Journal*, Vol. 31, No. 1, 1993, pp. 27–35.

[30]Wilcox, D. C., "Reassessment of the Scale-Determining Equation for Advanced Turbulence Models," *AIAA Journal*, Vol. 26, No. 11, 1988, pp. 1299–1310.

[31]Sarkar, S., Erlebacher, G., Hussaini, M. Y., and Kreiss, H. O., "The Analysis and Modelling of Dilatational Terms in Compressible Turbulence," *Journal of Fluid Mechanics*, Vol. 227, June 1991, pp. 473–493.

F. W. Chambers
Associate Editor